A fundamental viewpoint on the hydrogen spillover phenomenon of electrocatalytic hydrogen evolution

Jiayuan Li
Northwestern Polytechnical University
Jun Hu
Northwest University
Mingkai Zhang
Xi'an Jiaotong University
Wangyan Gou
Northwestern Polytechnical University
Sai Zhang
Northwestern Polytechnical University
Zhong Chen
Nanyang Technological University https://orcid.org/0000-0001-7518-1414
Yongquan Qu (yongquan@mail.xjtu.edu.cn)
Xi'an Jiaotong University https://orcid.org/0000-0002-6202-1929
Yuanyuan Ma
Northwestern Polytechnical University

Article

Keywords: Metal-supported Electrocatalysts, Interfacial Charge Accumulation, Hydrogen Transfer

Posted Date: December 2nd, 2020

DOI: https://doi.org/10.21203/rs.3.rs-103832/v1

Version of Record: A version of this preprint was published at Nature Communications on June 9th, 2021.
See the published version at https://doi.org/10.1038/s41467-021-23750-4.

Abstract

Hydrogen spillover phenomenon of metal-supported electrocatalysts can significantly impact their activity in hydrogen evolution reaction (HER). However, design of active electrocatalysts faces grand challenges due to the insufficient understandings on how to overcome this thermodynamically and kinetically adverse process. We theoretically profile that the interfacial charge accumulation induced by the large work function difference between metal and support ($\Delta\Phi$) and sequentially strong interfacial proton adsorption construct a high energy barrier for hydrogen transfer. Theoretical simulations and control experiments rationalize that small $\Delta\Phi$ induces interfacial charge dilution and relocation, thereby weakening interfacial proton adsorption and enabling efficient hydrogen spillover for HER. Experimentally, a series of Pt alloys-CoP catalysts with tailorable $\Delta\Phi$ showed a strong $\Delta\Phi$-dependent HER activity, in which PtIr/CoP with the smallest $\Delta\Phi$ = 0.02 eV delivered the best HER performance. These findings have conclusively identified $\Delta\Phi$ as the criterion in guiding the design of hydrogen spillover-based binary HER electrocatalysts.

Introduction

Hydrogen, featured by high gravimetric energy density and zero-emission, holds great potentials as the sustainable alternatives to fossil fuels.[1,2] Its promising application prospect has stimulated the intensive investigations to develop various methodologies for the scalable and cost-effective production of hydrogen.[3] Electrocatalytic water hydrolysis offers an attractive approach to generate hydrogen with high purity.[4] However, this technology is still far from being commercially competitive to the hydrogen production through steam reforming. The key issue is to look for the efficient and robust electrocatalysts to maximize the catalytic efficiency with high longevity under the operating conditions, especially for those in acidic electrolytes.[5,6]

Currently, catalyst design for electrocatalytic hydrogen evolution reaction (HER) is guided by the classic volcano theory in which hydrogen adsorption free energy (ΔG_H) on catalyst surface is used as an indicator of the catalytic efficiency.[7] In this theory, neither too strong nor too weak adsorption of active hydrogen species ($\Delta G_H \approx 0$) is recognized as the criterion for efficient HER electrocatalysts, since this state can facilitate both hydrogen adsorption and desorption.[7] Therefore, the design of electrocatalysts to be as closer as possible tothe “volcano” top is of intensive academic and industrial interest.[7,8] With this concept in mind, platinum (Pt)-based materials are advocated as the best candidates due to their near ideal ΔG_H.[9,10] Considering the scarcity of Pt in nature, various earth-abundant transition metal compounds (e.g. sulfides, phosphides, carbides and nitrides) as the alternatives have been explored.[11-16] Althoughthe significant progress has been made so far, the state-of-the-art inexpensive HER electrocatalysts still suffer from relatively low activity and poor durability. Especially in harsh acidic media, the deactivation is often observed under this corrosive conditions.[17,18] Thus, it calls for further exploitation of highly efficient, robust, and cost-effective HER electrocatalysts through conceptual innovation.

Inspired by the hydrogen spillover phenomenon in thermal hydrogenation through the strong metal-support interaction,[19,20] recently, hydrogen spillover has emerged as a new frontier in the binary metal/support HER electrocatalysts,[21-26] which undergoes (1) the strong proton adsorption on metals ($\Delta G_{H\text{-}metal} < 0$); (2) the interfacial hydrogen spillover from metals to supports and (3) efficient hydrogen desorption on supports ($\Delta G_{H\text{-}support} > 0$). This strategy affords a new concept by integrating both advantages of metal and support and thereby kinetically promotes the proton adsorption and hydrogen desorption. Also, this design conception is cost-effective as it canreduce the metal usage while still deliver the competitive catalytic performance.[22,24] Unfortunately, the successful cases based on this conception are still rare due to the lack of the fundamental understandings on what are the key factors behind the hydrogen spillover process, a thermodynamically and kinetically unfavorable process for HER. Thus, the fundamental understandings on how to enable energetically favorable hydrogen spillover under HER operating conditions are crucial to the design and synthesis of such hydrogen spillover-based binary (HSBB) catalysts.

Herein, by theoretically profiling the hydrogen spillover kinetics in such HSBB catalysts, the occurrence of the interfacial hydrogen spillover is predicted to be determined by the work function difference between metal and support ($\Delta\Phi$). Large value of $\Delta\Phi$ leads to interfacial charge accumulation, strong proton trapping at the interface and thereby unfavorable hydrogen spillover kinetics from metal to support during HER. Inspired by this finding, the modulation of work function of metal by alloying with a second metal to match that of the support provides a practical strategy to minimize the interfacial charge accumulation and enable efficient the interfacial hydrogen transfer. To examine our theoretical predictions, a suite of the alloyed Pt nanoparticles anchored on CoP (PtM/CoP, M = Rh, Pd, Ag, Ir and Au) were prepared as model catalysts to investigate the hydrogen spillover kinetics for HER, where the $\Delta\Phi$ was used as the criteria. We experimentally and theoretically demonstrated effective hydrogen spillover in PtIr/CoP due to their close work functions. The optimized Pt_2Ir_1/CoP with a low metal loading of 1.0 *wt*% delivered the superior HER performance with the small Tafel slope of 25.2 mV/dec, low overpotentials of 7 mV at 20 mA/cm^2 and nearly undecayed stability over a period of 500 h. Our finding not only provides deep insights on the hydrogen spillover phenomenon in HER electrocatalysts,but also offers a promising strategy to tackle this fundamental challenge and establishes a thorough conceptive grounding for the design of highly performed HER electrocatalysts.

Results And Discussion

Theoretical Viewpoint on the Hydrogen Spillover Phenomenon in Binary HER Electrocatalysts

Generally, the interaction between a metal and a support with the large difference in their Fermi energies (E_f) constructs a Schottky junction at the interface (Figure 1). Such a large difference in their E_f drives the interfacial charge flow until the system reaches an equilibrium, followed by the Schottky barrier formation and charge accumulation at the interface of metal and support, thus endowing the interfacially catalytic sites with the strong proton absorption ability.[27-29] In this case, the interfacial hydrogen spillover from

metal to support has to overcome a large energy barrier, leading to a kinetically difficult process and thereby unsatisfactory HER activity.

Conversely, when metal and support possess similar E_f, they should restrain the interfacial charge-transfer and minimize the interfacially accumulated charge (Figure 1). With this electronic configuration, the energy barrier for the interfacial hydrogen spillover is expected to be significantly declined, theoretically resulting in a high catalytic HER activity. Inspired by above rational analysis and the qualitative analysis for E_f by the work function (Φ) in materials,[30] we hypothesize that the difference in Φ between metal and support ($\Delta\Phi = |\Phi_{metal} - \Phi_{support}|$) plays a crucial role in determining the transfer kinetics of the interfacial hydrogen spillover. The minimized $\Delta\Phi$ theoretically would reduce the hydrogen spillover barrier, resulting in efficient HER catalysis. If this hypothesis can be validated, the key issue for such binary catalysts mentioned above will be revealed accordingly and an enormous amount of time and expenses for catalyst design or selection will be saved through simply examining the $\Delta\Phi$ between the two components in the HSBB electrocatalysts.

Rational Design of PtM/CoP Model Catalysts

Taking Pt/CoP as a model catalyst, the $\Delta\Phi$ of ~ 0.19 eV between Pt (Φ_{Pt} = 5.37 eV) and CoP (Φ_{CoP} = 5.56 eV) induces a large energy barrier for hydrogen spillover from Pt to CoP and thereby delivers no synergistic enhancements in the catalytic HER activity (Figure S1 and S2), consistent with our previous report.[22] According to the above analysis, the small $\Delta\Phi$ is expected to realize efficient hydrogen spillover, if Φ of either metal or support can be tailorable. Practically, the energy-level configuration of a metal can be precisely modulated by alloying with another metal.[31,32] Thus, alloying Pt is an effective strategy to regulate $\Delta\Phi$ between metal and CoP substrate.

Based on the principle that alloying between the neighbors in periodic table of elements is easy to happen without structural aberration, various foreign metals (M = Ir, Rh, Pd, Ag and Au) with the period/group adjacent to Pt come into sight. Compared to that of CoP, the calculated values of Φ for PtIr, PtRh, PtPd, PtAg and PtAu were 5.54 eV, 5.33 eV, 5.40 eV, 5.18 eV and 5.34 eV, respectively (Figure 2 and S1), indicating that PtIr/CoP might be the best candidate to achieve the kinetically favorable hydrogen spillover from metal to CoP and further comparing with other PtM/CoP model catalysts offer an opportunity to examine our viewpoint.

Synthesis, Characterizations, and Catalytic Performance

Accordingly, Pt/CoP, PtAg/CoP, PtRh/CoP, PtAu/CoP, PtPd/CoP and PtIr/CoP electrocatalysts were synthesized through the same method (details can be found in Methods section). To confirm the successful preparation, powder X-ray diffraction (XRD) curves of PtIr/CoP with a metal loading of 1.0 *wt*% and a Pt/Ir molar ratio of 2 : 1 (determined by inductively-coupled plasma mass spectrometry, ICP-MS, Table S1) are shown in Figure 3a as an example. The pattern is consistent with that of CoP standard (JCPDS #29-0497), suggesting unaltered phase of CoP during synthesis.[33] No XRD peaks of the loaded

metal were observed due to the small size and low loading in the catalysts. The transmission electron microscopy (TEM) image (Figure 3b) confirms the uniform distribution of the small PtIr alloyed metal nanoparticles of ~ 1.60 nm on CoP nanosheets. The magnified TEM image in Figure 3c shows the interplanar spacings of 2.25 and 2.82 Å, corresponding to the respective (111) facet of Pt alloy with cubic lattice and the (011) facet of CoP with orthorhombic lattice. In the high-resolution X-ray photoelectron spectra (XPS) of PtIr/CoP (Figure S3), the typical signals of CoP, Pt and Ir species were identified.[34-36] Considering the binding energy of Pt $4f_{7/2}$ (71.0 eV) and Ir $4f_{7/2}$ (60.8 eV) in Pt^0 and Ir^0 benchmarks, a shift to higher binding energy for Pt $4f_{7/2}$ (71.2 eV) together with a shift to a lower value for Ir $4f_{7/2}$ (60.4 eV) in the case of PtIr/CoP were related to a lower electron density on the Pt due to the presence of Ir with the relatively higher electron affinity, suggesting the formation of a bimetallic PtIr alloy.[35,37] Energy-dispersive X-ray (EDX) mapping and line scan (Figure 3c) for PtIr/CoP suggest uniform distribution of Co and P elements in nanosheets and concentrated distribution of Pt and Ir elements in nanoparticles, further confirming the formation of PtIr/CoP hybrids.

To experimentally explore the fundamental electrocatalytic behavior of the above model catalysts, we carried out the linear sweep voltammetry (LSV) *via* a standard three-electrode system in 0.5 M H_2SO_4 solution. In line with the previously reported protocols, all overpotentials here were iR-corrected and calibrated to the reversible hydrogen electrode (RHE) scale (see Supplementary Information for details). Initially, the catalytic performance of various PtIr/CoP electrocatalysts with different molar ratios of Pt/Ir was evaluated. As shown in Figure S4 and Table S1, the Pt_3Ir_1/CoP, Pt_2Ir_1/CoP, Pt_1Ir_1/CoP, Pt_1Ir_2/CoP, and Pt_1Ir_3/CoP electrocatalysts showed similar structural features and chemical compositions. The V-shaped relationship between the HER activity and the Pt/Ir molar ratio revealed that the best catalytic HER performance was observed on Pt_2Ir_1/CoP (Figure S5). Afterwards, the loadings of Pt_2Ir_1/CoP were assessed. It was recognized that the chemical and morphological characters, especially the size of the loaded metal in Pt_2Ir_1/CoP with various metal loadings (from 0.5 to 2.0 *wt*%) were similar (Figure 3a and S6 and Table S2), therefore their influences can be excluded. Revealed from the catalytic evaluation (Figure S7), the Pt_2Ir_1/CoP showed evident activity improvement with the increase of metal loadings. It should be noted that such loading increment reached a threshold (herein, 1.0 *wt*%) and afterwards delivered the limited activity improvement, suggesting an optimum metal loading at 1.0 *wt*%.

To experimentally examine the above the proposed fundamental understandings on the hydrogen spillover phenomenon, Pt_2Ag_1/CoP, Pt_2Rh_1/CoP, Pt_2Au_1/CoP, Pt/CoP, Pt_2Pd_1/CoP and Pt_2Ir_1/CoP catalysts with the same metal loading of 1.0 *wt*% were synthesized and evaluated for HER (If not otherwise specified, all Pt_2M_1/CoP catalysts correspond to the metal loading of 1.0 *wt*%). As shown in Figure S8 and Table S3, all catalysts exhibited nearly the same structural features including metal sizes, morphologies and phases of catalysts, which enables a straightforward comparison of their electrocatalytic performance only by considering the chemical composition of the alloyed metals.

As predicted for the most promising model catalyst, the Pt_2Ir_1/CoP catalysts delivered the highest catalytic activity with the lowest overpotential (h_{20}) of 7 mV at 20 mA•cm^{-2} and the smallest Tafel slope

of 25.2 mV/dec (Figure 4a and 4b), which comprehensively surpassed the commercial benchmarks and the most of the state-of-the-art HER electrocatalysts (Table S4 and S5). Especially, by normalizing to the noble-metal weight loading, the Pt_2Ir_1/CoP catalysts gave a mass activity as high as 110 A•mg_{PtIr}^{-1} at overpotential of -50 mV *vs* RHE, which was 78 times higher than that of the commercial HER catalyst (20 *wt*% Pt/C, 1.4 A•mg_{Pt}^{-1}) and even an order of magnitude higher than that for the state-of-the-art noble-metal HER electrocatalysts under the similar operation conditions (Figure 4c).[21,23,26,38-51] This value represents the highest noble-metal utilization activity for HER so far, demonstrating the importance of our primary understandings on the hydrogen spillover of binary metal/support catalysts.

The Pt_2Ir_1/CoP also displayed extremely high catalytic HER durability without an obvious decay for 50000 cycles as well as a period of 500 h (Figure 4d). The characterizations, including XPS, ICP-MS and HRTEM of the spent Pt_2Ir_1/CoP-1.0 electrocatalysts after the durability test (Figure S9 and S10), indicate that the structure and composition underwent negligible changes. Also, the negligible Faraday efficiency loss was observed for Pt_2Ir_1/CoP during HER (inset in Figure 4d). These results demonstrate the catalytic robustness of Pt_2Ir_1/CoP towards HER and their potentials for practical applications.

Correlation between $\Delta\Phi$ and HER Activity

To gain further insights on the relationship between the $\Delta\Phi$ and HER activity of the above catalysts, the activity parameters (h_{20} and Tafel slopes) of the six prepared electrocatalysts were compared as a function of $\Delta\Phi$ (Figure 5a and 5b). The plots of the observed h_{20} and $\Delta\Phi$ values of various catalysts displayed a nearly linear decreasing trend, which could be expressed as $h_{20} = 16.2 + 470.5\ \Delta\Phi$. The derived Tafel slopes of various electrocatalysts exhibited a linear increasing trend as the function of $\Delta\Phi$, expressed as *Tafel slope* = $21.3 + 324.8\ \Delta\Phi$. Both plots representatively demonstrated the highest activity of Pt_2Ir_1/CoP because of the fastest kinetics in the linear trend at the minimum $\Delta\Phi$ value of ~ 0.02 eV. As a comparison, the initial Pt/CoP with median $\Delta\Phi$ of ~ 0.19 eV corresponded to the mediocre activity and kinetics. In summary, our observations confirm the strong dependence of the $\Delta\Phi$ values of various PtM/CoP on their HER catalytic activity.

To further understand this relationship, the h_{20} and Tafel slopes of Pt/CoP and Pt_2Ir_1/CoP catalysts with various metal loading were compared (Figure 5c and 5d). By increasing Pt loading from 0.5 *wt*% to 2.0 *wt*%, the above activity parameters of Pt/CoP showed little variation compared with those of bare CoP (h_{20} = 156 mV and Tafel slope = 108.1 mV•dec^{-1}). Clearly, the CoP acts as the dominant catalytical active species and the kinetic bottleneck of hydrogen adsorption remains,[22,52] probably due to the intrinsically large barrier of interfacial hydrogen spillover. Comparatively, the quickly decreased h_{20} and Tafel slopes of Pt_2Ir_1/CoP with the increase of metal loadings suggest a synergistic HER mechanism between the loaded alloys and CoP, leading to the kinetically favorable process. Considering such low metal loadings in the series catalysts of Pt_2Ir_1/CoP and the limited contributions of loaded metalsto the solo HER (Figure S11), the promoted hydrogen spillover from Pt with the Ir incorporation to CoP is a most

facile approach to realize both the beneficial proton adsorption on the alloyed PtIr and the easy hydrogen desorption on CoP and thus overcome the kinetic bottleneck for hydrogen production.[21,22]

The kinetics of HER processes on the bare CoP, Pt/CoP and Pt_2Ir_1/CoP was further evaluated by electrochemical impedance spectroscopy (EIS) at different overpotentials (Figure S12). The recorded Nyquist plots were simulated by a double-parallel equivalent circuit model (insets of Figure S12 and Table S6).[53-55] The first parallel components (T and R_1) reflect the charge-transfer kinetics. The small values of potential-independent R_1 for all catalysts suggested CoP as a good conductive network in catalysts and thereby created a fast charge-transfer kinetics for HER.

The second parallel components (C and R_2) describe the hydrogen adsorption behavior on the catalyst surface, where R_2 and C represent the hydrogen adsorption resistance and pseudo-capacitance, respectively. Considering the potential-dependent R_2 for all catalysts,it is rational to quantify their hydrogen adsorption kinetics *via* plotting log R_2 *vs.* overpotential and calculating the EIS-derived Tafel slopes by virtue of the Ohm's law.[55] As shown in Figure 5e, the similar EIS-derived Tafel slope of Pt/CoP compared with those of bare CoP suggestsits unaltered hydrogen adsorption kinetics. Hence, Pt/CoP showed the individual hydrogen adsorption on respective Pt and CoP, suggesting the failure of the interfacial hydrogen spillover from Pt to CoP due to the sluggish spillover kinetics. Comparatively, the significantly declined EIS-derived Tafel slope for Pt_2Ir_1/CoP indicates an accelerated hydrogen adsorption kinetics. Such phenomenon revealed that the intrinsically insufficient hydrogen adsorption on CoP was facilitated by merging a successful hydrogen spillover from metal to CoP as a new faster pathway for hydrogen intermediate (H*) supply owing to the profoundly enhanced spillover kinetics (better than the kinetics of solo hydrogen adsorption on CoP).

To further examine this point, the apparent activation energy and order of reaction for the overall HER process on Pt_2Ir_1/CoP were investigated (Figure 5f). The measured activation energy of 20.9 kJ•mol^{-1} and reaction order of ~ 1.98 were derived from the temperature- and pH-dependent relation and the extrapolation of LSV curves of HER (Figure S13), which also fell in the domain of the previously reported HSBB electrocatalysts in acid media.[21,23,26] This coincidence further supports the successful hydrogen spillover process in Pt_2Ir_1/CoP and its contribution to the significantly improved HER activity with a much low metal loading.

Overall, $\Delta\Phi$ is experimentally verified as the index linked to the energy barrier of the interfacial hydrogen spillover between metals and supports in HER, in which the small value of $\Delta\Phi$ suggests anenergetically favorable HER kinetics in the HSBB electrocatalysts.

Theoretical Modelling of Hydrogen Spillover in Pt_2Ir_1/CoP

To better understand the fundamental efficacy of $\Delta\Phi$, density functional theory (DFT) calculations were performed to elucidate how hydrogen spillover contributes to the overall HER activity and how $\Delta\Phi$ affects the interfacial electronic states and kinetics of the interfacial hydrogen spillover. Accordingly, the energy

profiles on the Pt/CoP and Pt_2Ir_1/CoP catalysts were compared (Figure 6a and 6b). Details of the simulation models and methods are found in Supplementary Information. On the Pt/CoP surface, the H* preferentially adsorbed at Pt with ΔG_H values of -0.20 eV (site 1), -0.06 eV (site 2) and -0.36 eV (site 3), respectively, suggesting significant proton trapping at the interface of Pt and CoP (site 3). Conversely, the ΔG_H for the most stable Co site (site 4) was 0.04 eV, indicating that Co site of CoP was superior to produce a hydrogen molecule by breaking the bond of Co–H. If the H can transfer across the edge of the Pt cluster to the CoP surface, the HER will be easy to proceed for both the initial adsorption of a proton and final desorption of H_2. However, such a spillover process is hindered at the interface due to the strong hydrogen capturing at the site 3 (ΔG_H = -0.36 eV). Therefore, the overall HER process is limited by the diffusion of active hydrogen species across the interface from site 3 to site 4 with the significant thermodynamic (0.40 eV) and kinetics barrier (0.79 eV).

In Pt_2Ir_1/CoP, it is noted that H* adsorption on Co top (site 4', 0.05 eV) is close to the case in Pt/CoP because these Co sites are far away from PtIr alloys. Also, the changes in the ΔG_H on site 1' and site 2' range from -0.20 eV to -0.39 eV and from -0.06 eV to -0.15 eV, respectively, suggesting an increased hydrogen adsorption at the metal sites. Importantly, the significant changes of ΔG_H at the interface (site 3') from -0.36 eV to -0.08 eV indicates the gradually moderate hydrogen adsorption that can induce the greatly decreased thermodynamic (0.13 eV) and kinetics barrier (0.39 eV) from site 3' to site 4'. In this regard, the hydrogen spillover across the interface is greatly facilitated on the Pt_2Ir_1/CoP surface, leading to a highly efficient HER activity.

Starting from the electronic structures, we seek to further understand the relationship between the hydrogen spillover across the interface of PtIr and CoP and the $\Delta \Phi$ of binary components. The electron density difference (EDD) mapping for Pt/CoP and Pt_2Ir_1/CoP is shown in Figure 5c. It is found that the high-density electroncloud is concentrated at the interface for Pt/CoP system. Generally, active hydrogen species with the unsaturated electrons on 1s orbital is easily trapped at the electron-rich region.[56] Therefore, the electron accumulation at the interface of Pt and CoP, due to the large difference in their work functions, brings a strong bond between proton and interfacial sites, thus limiting the interfacial hydrogen spillover. Comparatively, the introduction of Ir into Pt triggers a significant relocalization of electrons, which is characterized by the vanish of the interfacially concentrated electron-cloud and directionally migrated electron-cloud towards Ir and CoP sublayer. The diluted electron-cloud at the interface of Pt_2Ir_1/CoP is highly consistent with the view that the small $\Delta \Phi$ can restrain the interfacial charge-transfer and minimize the interfacial electron accumulation. Such phenomena in the interfacial charge states of two catalysts are also verified by their XPS profiles (Figure S14). Consequently, the hydrogen adsorption atinterface site (site 3') in Pt_2Ir_1/CoP was significantly weakened and gradually became thermo-neutral, which could serve as the mediators for interfacial hydrogen spillover. Furthermore, the migrated electron-cloud towards Ir will enhance the hydrogen adsorption on the Pt sites adjacent to Ir (site 1' and site2') in Pt_2Ir_1/CoP and thus facilitate the H* accumulation on Pt, finally boosting the interfacial hydrogen spillover.

Therefore, the nature of $\Delta\Phi$ between metals and supports and its contribution to HER performance are mainly embodied in two aspects (Figure 7). **(a) $\Delta\Phi$ affects the interfacial charge accumulation.** Replacing Pt by PtIr alloy in Pt/CoP system will offset the intrinsic $\Delta\Phi$ between two components of the interface and thus restrain the interfacial charge flow, resulting in the reduced charge accumulation at the interface. This then enables the interfacial sites with the thermo-neutral hydrogen adsorption to become the mediators for the energetically favorable interfacial hydrogen spillover. With these functions enabled, the energy barrier for interfacial hydrogen spillover will be significantly reduced and a hydrogen spillover channel of PtIr→interface→CoP is formed. **(b) $\Delta\Phi$ induces the surface charge relocation.** The small $\Delta\Phi$ of binary components in PtIr/CoP results in the charge redistribution, eventually forming an electron enrichment region on metals and CoP instead of the interface. This character endows the enhanced proton adsorption on the alloyed metal sites, which is also beneficial for the interfacial hydrogen spillover. For these reasons, a high performance binary PtIr/CoP HER electrocatalysts are realized with a close work function, which have displayed strong hydrogen adsorption on PtIr, energetically favorable hydrogen spillover (PtIr→interface→CoP), and the efficient hydrogen desorption on CoP. All these features correspond well to our fundamental understandings on the design of HSBB catalysts. The novel concept of establishing advanced HER electrocatalysts through engineering the critical parameter of $\Delta\Phi$ has been substantiated through both experiments and simulations.

Conclusions

In summary, we theoretically and experimentally demonstrate that the work function difference between metal and support determines the interfacial electronic structures of a binary metal-supported HER electrocatalyst and thereby influences the interfacial hydrogen spillover from metal to support. Small $\Delta\Phi$ dilutes the interfacial charge density and relocates the electrons to metal and support, leading to the weakened proton adsorption at the interface and enhanced proton adsorption on metals. Thus, the significantly declined energy barrier for hydrogen transfer across the interface of metal and support enables the superior catalytic performance for HER. The hypothesis was experimentally confirmed by a series of Pt alloys-CoP hybrids with the tailorable $\Delta\Phi$, in which Pt_2Ir_1/CoP (1.0 *wt.*%) with the smallest $\Delta\Phi$ value exhibited the best HER performance, even better than the majority of the state-of-the-art Pt-based HER electrocatalysts as well as the commercially available Pt/C (20 *wt.*%). Our findings have not only improved the atomic understandings on the hydrogen spillover phenomenon for HER, but also pointed out a new design strategy towards high performance HER electrocatalysts.

Methods

Synthesis of CoP support. $Co(OH)_2$ nanosheetswere synthesized *via* a similar process in previous reports. Typically, 0.582 g of $Co(NO_3)_2{\cdot}6H_2O$ and 0.56 g of hexamethylenetetramine (HMT) were dissolved in 15 mL of distilled water under the vigorous stirring to form a clear solution. The solution then was transferred into a 20 mL Teflon-lined stainless-steel autoclave. The autoclave was placed into an electric oven at 100 °C for 10 h. After cooling to room temperature naturally, $Co(OH)_2$ nanosheets werecollected

by centrifugation, and washed with water/ethanol alternatively and driedunder vacuum. To prepare CoP nanosheets, $Co(OH)_2$ nanosheets (100 mg) and $NaH_2PO_2·H_2O$ (2 g) were put at two separate positions in a quartz boat with NaH_2PO_2 at the upstream side of the furnace. Subsequently, the temperature of the tube furnace was raised to 300 °C with a ramping rate of 5 °C•min^{-1} andmaintained at 300 °C for 60 min, and then naturally cooled to room temperature under the protection of Ar gas with a flow rate of 100 mL•min^{-1}.

Synthesis of PtM/CoP model catalysts. Various PtM/CoP catalysts studied here were synthesized using an *in-situ* chemical reduction of metal-salt precursors. Taking the synthesis of PtIr/CoP as an example: 50 mg of CoP was suspended in 47 ml of distilled water, and then x μL (where x = 50, 100, 150 and 200) mixture of H_2PtCl_6 (Pt content = 5 mg•mL^{-1}) and $IrCl_3$ (Ir content = 5 mg•mL^{-1}) solution with the desired molar ratio“y” (where y = $[Pt^{4+}]/([Ir^{3+}])$, and y = 3, 2, 1, 0.5 and 0.33) was added to achieve the theoretical Pt : Ir molar ratio of 3 : 1, 2 : 1, 1 : 1, 1 : 2 and 1 : 3 as well as the metal loadings of 0.5 *wt*%, 1.0 *wt*%, 1.5 *wt*% and 2.0 *wt*%. Subsequently, 3 mL of the freshly prepared $NaBH_4$ aqueous solution (containing 95 mg $NaBH_4$) was quickly added under vigorous stirring. After 3 h reaction under stirring, the products were collected through centrifuging, washed with water/ethanol thoroughly and then dried at 60 °C for 12 h under vacuum to obtain the PtIr/CoP catalysts. Other PtM/CoP catalysts can be obtained *via* the similar process when replacing the $IrCl_3$ solution by other metal-salt solution (metal content = 5 mg•mL^{-1}), such as $RhCl_3$, $PdCl_3$, $AgNO_3$ and $AuCl_3$.

Characterization. Ultraviolet photoemission spectroscopy was also carried out on an ESCALAB 250 Xi spectrometer using He_I resonance lines (21.2 eV). ICP-MS was performed on an Agilent ICPMS 7500CE. Powder XRD data were acquired on a Shimadzu X-ray diffractometer with Cu Kα radiation. TEM and EDX measurements were performed on a JEOL 2100F TEM with an accelerating voltage of 200 kV. XPS measurements were carried out on a Thermo Electron Model with Al Kα as the excitation source.

References

1 Turner, J. A. Sustainable hydrogen production. *Science* **305**, 972-974 (2004).

2 Lewis, N. S. & Nocera, D. G. Powering the planet: chemical challenges in solar energy utilization. *Proc. Nati. Acad. Sci.* **103**, 15729-15735 (2006).

3 Dresselhaus, M. & Thomas, I. Alternative energy technologies. *Nature* **414**, 332-337 (2001).

4 Chu, S. & Majumdar, A. Opportunities and challenges for a sustainable energy future. *Nature* **488**, 294-303 (2012).

5 Jiao, Y., Zheng, Y., Jaroniec, M. & Qiao, S. Z. Design of electrocatalysts for oxygen-and hydrogen-involving energy conversion reactions. *Chem. Soc. Rev.* **44**, 2060-2086 (2015).

6 McCrory, C. C. L. *et al.* Benchmarking hydrogen evolving reaction and oxygen evolving reaction electrocatalysts for solar water splitting devices. *J. Am. Chem. Soc.* **137**, 4347-4357 (2015).

7 Seh, Z. W. *et al.* Combining theory and experiment in electrocatalysis: insights into materials design. *Science* **355**, eaad4998 (2017).

8 Zheng, Y., Jiao, Y., Jaroniec, M. & Qiao, S. Z. Advancing the electrochemistry of the hydrogen-evolution reaction through combining experiment and theory. *Angew. Chem. Int. Edit.* **54**, 52-65 (2015).

9 Greeley, J., Jaramillo, T. F., Bonde, J., Chorkendorff, I. & Nørskov, J. K. Computational high-throughput screening of electrocatalytic materials for hydrogen evolution. *Nat. Mater.* **5**, 909-913 (2006).

10 Li, M. *et al.* Single-atom tailoring of platinum nanocatalysts for high-performance multifunctional electrocatalysis. *Nat. Catal.* **2**, 495-503 (2019).

11 Roger, I., Shipman, M. A. & Symes, M. D. Earth-abundant catalysts for electrochemical and photoelectrochemical water splitting. *Nat. Rev. Chem.* **1**, 0003 (2017).

12 Voiry, D., Shin, H. S., Loh, K. P. & Chhowalla, M. Low-dimensional catalysts for hydrogen evolution and CO_2 reduction. *Nat. Rev. Chem.* **2**, 0105 (2018).

13 Wang, H. & Gao, L. Recent developments in electrochemical hydrogen evolution reaction. *Curr. Opin. Electrochem.* **7**, 7-14 (2018).

14 Wang, J., Xu, F., Jin, H., Chen, Y. & Wang, Y. Non-noble metal-based carbon composites in hydrogen evolution reaction: fundamentals to applications. *Adv. Mater.* **29**, 1605838 (2017).

15 Zhao, G., Rui, K., Dou, S. X. & Sun, W. Heterostructures for electrochemical hydrogen evolution reaction: a review. *Adv. Funct. Mater.* **28**, 1803291 (2018).

16 Gao, M.-R., Chan, M. K. Y. & Sun, Y. Edge-terminated molybdenum disulfide with a 9.4-Å interlayer spacing for electrochemical hydrogen production. Nat. Commun. 6, 7493 (2015).

17 Ledendecker, M. *et al.* Stability and activity of non-noble-metal-based catalysts toward the hydrogen evolution reaction. *Angew. Chem. Int. Edit.* **56**, 9767-9771 (2017).

18 Masa, J., Andronescu, C. & Schuhmann, W. Electrocatalysis as the nexus for sustainable renewable energy: the gordian knot of activity, stability, and selectivity. *Angew. Chem. Int. Edit.* **59**, 15298-15312 (2020).

19 Prins, R. Hydrogen spillover. facts and fiction. *Chem. Rev.* **112**, 2714-2738 (2012).

20 Karim, W. *et al.* Catalyst support effects on hydrogen spillover. *Nature* **541**, 68-71 (2017).

21 Zhu, L. *et al.* A rhodium/silicon co-electrocatalyst design concept to surpass platinum hydrogen evolution activity at high overpotentials. *Nat. Commun.* **7**, 12272 (2016).

22 Li, J. *et al.* Ethylene-glycol ligand environment facilitates highly efficient hydrogen evolution of Pt/CoP through proton concentration and hydrogen spillover. *Energy Environ. Sci.* **12**, 2298-2304 (2019).

23 Sheng, M. *et al.* Approaching the volcano top: iridium/silicon nanocomposites as efficient electrocatalysts for the hydrogen evolution reaction. *ACS Nano* **13**, 2786-2794 (2019).

24 Liu, T. *et al.* Selective loading of atomic platinum on a $RuCeO_x$ support enables stable hydrogen evolution at high current densities. *Angew. Chem. Int. Edit.* **59**, 1-6 (2020).

25 Huang, J. *et al.* Boosting hydrogen transfer during volmer reaction at oxides/metal nanocomposites for efficient alkaline hydrogen evolution. *ACS Energy Lett.* **4** (2019).

26 Cheng, Y. *et al.* Rh/MoS_2 nanocomposite catalysts with Pt-like activity for hydrogen evolution reaction. *Adv. Funct. Mater.* **27**, 1700359 (2017).

27 Zhuang, Z. *et al.* $MoB/g\text{-}C_3N_4$ Interface materials as a schottky catalyst to boost hydrogen evolution. *Angew. Chem. Int. Edit.* **57**, 496-500 (2018).

28 Guo, L.-T. *et al.* Multifunctional Au–Co@CN nanocatalyst for highly efficient hydrolysis of ammonia borane. *ACS Catal.* **5**, 388-392 (2015).

29 Xue, Z.-H. *et al.* Janus Co/CoP nanoparticles as efficient Mott–Schottky electrocatalysts for overall water splitting in wide pH range. *Adv. Energy Mater.* **7**, 1602355 (2017).

30 Liu, J. *et al.* Metal-free efficient photocatalyst for stable visible water splitting via a two-electron pathway. *Science* **347**, 970 (2015).

31 Fain, S. C. & McDavid, J. M. Work-function variation with alloy composition: Ag-Au. *Phys. Rev. B* **9**, 5099-5107 (1974).

32 Kornblum, L., Shekhter, P., Slovatizky, Y., Amouyal, Y. & Eizenberg, M. Composition and crystallography dependence of the work function: experiment and calculations of Pt-Al alloys. *Phys. Rev. B* **86**, 125305 (2012).

33 Tang, C. *et al.* Fe-doped CoP nanoarray: a monolithic multifunctional catalyst for highly efficient hydrogen generation. *Adv. Mater.* **29**, 1602441 (2017).

34 Feng, J.-X., Tong, S.-Y., Tong, Y.-X. & Li, G.-R. Pt-like hydrogen evolution electrocatalysis on PANI/CoP hybrid nanowires by weakening the shackles of hydrogen ions on the surfaces of catalysts. *J. Am. Chem. Soc.* **140**, 5118-5126 (2018).

35 Ledesma, B., Juárez, J., Mazarío, J., Domine, M. & Beltramone, A. Bimetallic platinum/iridium modified mesoporous catalysts applied in the hydrogenation of HMF. *Catal. Today*, doi: j.cattod.2019.06.037 (2019).

36 Zhang, G. *et al.* Highly active and stable catalysts of phytic acid-derivative transition metal phosphides for full water splitting. *J. Am. Chem. Soc.* **138**, 14686-14693 (2016).

37 Wakisaka, M. *et al.* Electronic structures of Pt–Co and Pt–Ru alloys for CO-tolerant anode catalysts in polymer electrolyte fuel cells studied by EC–XPS. *J. Phys. Chem. B* **110**, 23489-23496 (2006).

38 Chen, Z. *et al.* Interface confined hydrogen evolution reaction in zero valent metal nanoparticles-intercalated molybdenum disulfide. *Nat. Commun.* **8**, 14548 (2017).

39 Luo, J., Zhang, L., Han, L., Liu, H. & Liu, X. Potential-cycling synthesis of single Pt atoms for efficient hydrogen evolution in neutral media. *Angew. Chem. Int. Edit.* **56**, 13694 –13698 (2017).

40 Jiang, K. *et al.* Single platinum atoms embedded in nanoporous cobalt selenide as electrocatalyst for accelerating hydrogen evolution reaction. *Nat. Commun.* **10**, 1743 (2019).

41 Yin, X.-P. *et al.* Engineering the coordination environment of single-atom platinum anchored on graphdiyne for optimizing electrocatalytic hydrogen evolution. *Angew. Chem. Int. Edit.* **57**, 9382-9386 (2018).

42 Xu, G.-R. *et al.* Polyallylamine-functionalized platinum tripods: enhancement of hydrogen evolution reaction by proton carriers. *ACS Catal.* **7**, 452-458 (2016).

43 Zhang, J. *et al.* Single platinum atoms immobilized on an MXene as an efficient catalyst for the hydrogen evolution reaction. *Nat. Catal.* **1**, 985-992 (2018).

44 Xu, J. *et al.* Boosting the hydrogen evolution performance of ruthenium clusters through synergistic coupling with cobalt phosphide. *Energy Environ. Sci.* **11**, 1819-1827 (2018).

45 Cheng, N. *et al.* Platinum single-atom and cluster catalysis of the hydrogen evolution reaction. *Nat. Commun.* **7**, 13638 (2016).

46 Liu, D. *et al.* Atomically dispersed platinum supported on curved carbon supports for efficient electrocatalytic hydrogen evolution. *Nat. Energy* **4**, 512-518 (2019).

47 Li, C. *et al.* Polyvinylpyrrolidone-coordinated single-site platinum catalyst exhibits high activity for hydrogen evolution reaction. *Angew. Chem.* **132**, 16036-16041 (2020).

48 Ye, S. *et al.* Highly stable single Pt atomic sites anchored on aniline-stacked graphene for hydrogen evolution reaction. *Energy Environ. Sci.* **12**, 1000-1007 (2019).

49 Zhang, H. *et al.* Dynamic traction of lattice-confined platinum atoms into mesoporous carbon matrix for hydrogen evolution reaction. *Sci. Adv.* **4**, eaao6657 (2018).

50 Xu, J. *et al.* Amorphous MoO_X-stabilized single platinum atoms with ultrahigh mass activity for acidic hydrogen evolution. *Nano Energy* **70**, 104529 (2020).

51 Tiwari, J. N. *et al.* Multicomponent electrocatalyst with ultralow Pt loading and high hydrogen evolution activity. *Nat. Energy* **3**, 773-782 (2018).

52 Kong, D. *et al.* Synthesis of MoS_2 and $MoSe_2$ films with vertically aligned layers. *Nano Lett.* **13**, 1341-1347 (2013).

53 Šimpraga, R., Tremiliosi-Filho, G., Qian, S. & Conway, B. In situ determination of the 'real are factor' in H_2 evolution electrocatalysis at porous Ni-Fe composite electrodes. *J. Electroanal. Chem.* **424**, 141-151 (1997).

54 Krstajić, N., Grgur, B., Mladenović, N., Vojnović, M. & Jaksić, M. The determination of kinetics parameters of the hydrogen evolution on Ti-Ni alloys by ac impedance. *Electrochim. Acta* **42**, 323-330 (1997).

55 Damian, A. & Omanovic, S. Ni and Ni-Mo hydrogen evolution electrocatalysts electrodeposited in a polyaniline matrix. *J. Power Sources* **158**, 464-476 (2006).

56 Janotti, A. & Van de Walle, C. G. Hydrogen multicentre bonds. *Nat. Mater.* **6**, 44-47 (2007)

Declarations

Acknowledgements: We acknowledge the financial support from China Postdoctoral Science Foundation (2018M640994 and 2018T111034) and National Nature Science Foundation of China (Grants 21872109, 21603170, 91645203). Y. Qu is supported by the Cyrus Tang Foundation through Tang Scholar program. J. Li is supported by Postdoctoral Innovative Talents Support program (BX20180246) and Young talent Support project of Shannxi(20200601). Y. Ma is supported byNational Natural Science Foundation of Shaanxi province, China (No. 2020JM-039). Jun Hu also acknowledges the financial support from the National Natural Science Foundation of China (No. 21676216), National Natural Science Foundation of Shaanxi province, China (No. 2019JM-294) and Special Project of Shaanxi Provincial Education Department (No. 20JC034).

Author Information Correspondence and requests for materials should be addressed to Y. Q. (yongquan@mail.xjtu.edu.cn), J. H. (hujun32456@163.com), Y. Y. (yyma@nwpu.edu.cn).

Figures

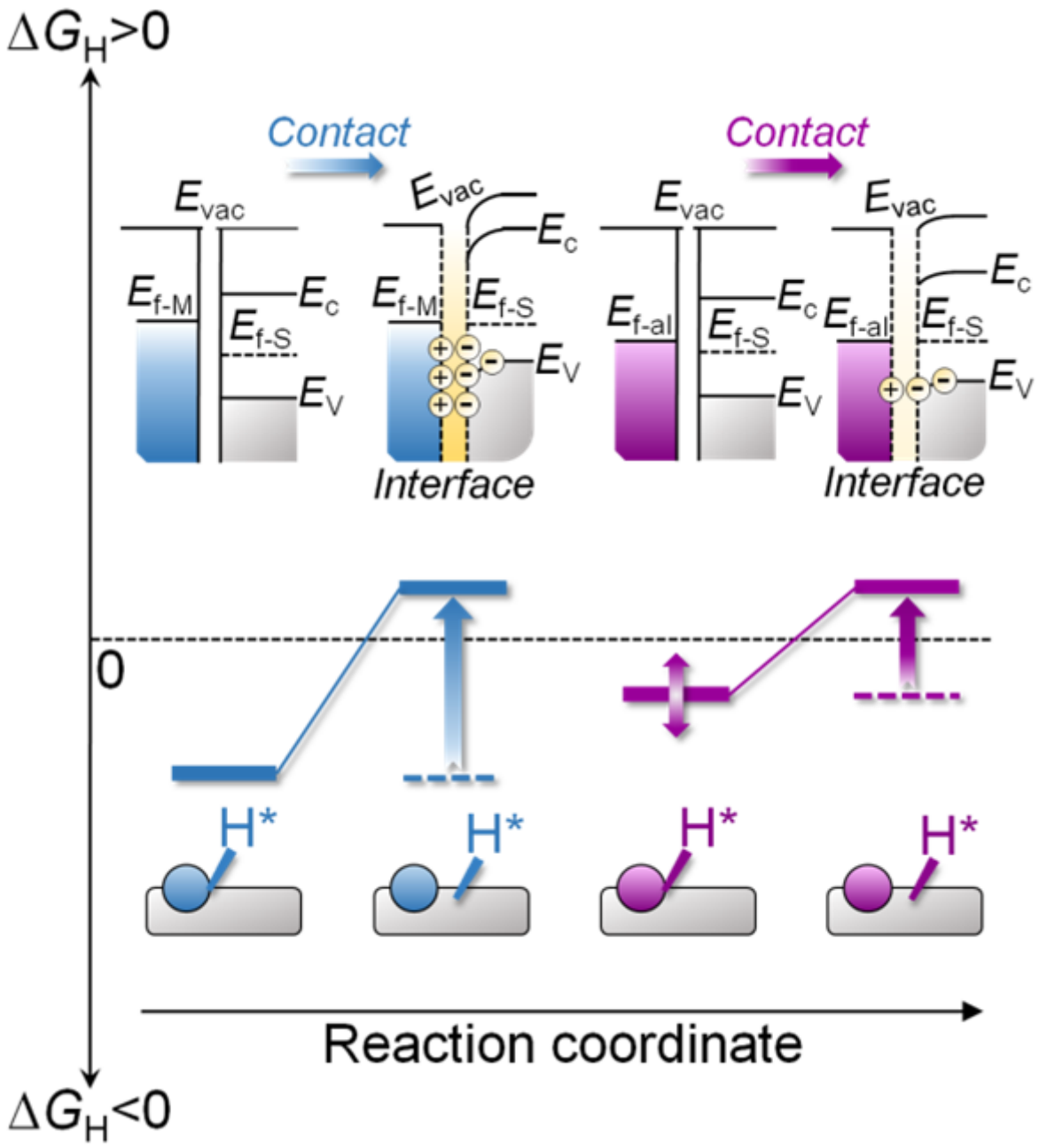

Figure 1

Schematic illustrations of the interfacial electronic configurations and hydrogen spillover phenomenon in HSBB catalysts. Evac = vacuum energy, Ec = conduction band, Ev = valence band, Ef-M = Fermi level of metal, Ef-al = Fermi level of alloy, Ef-S = Fermi level of support.

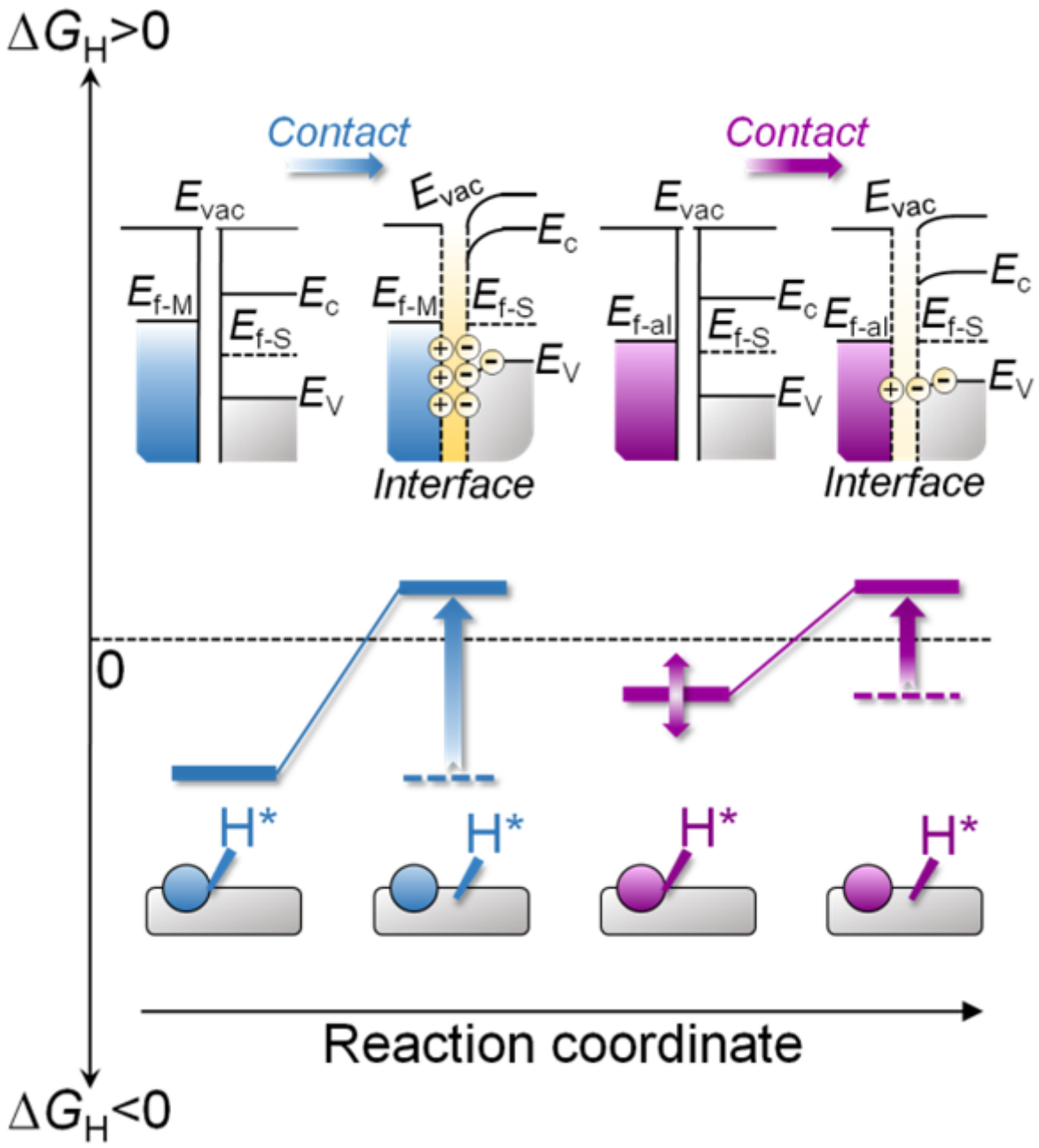

Figure 1

Schematic illustrations of the interfacial electronic configurations and hydrogen spillover phenomenon in HSBB catalysts. Evac = vacuum energy, Ec = conduction band, Ev = valence band, Ef-M = Fermi level of metal, Ef-al = Fermi level of alloy, Ef-S = Fermi level of support.

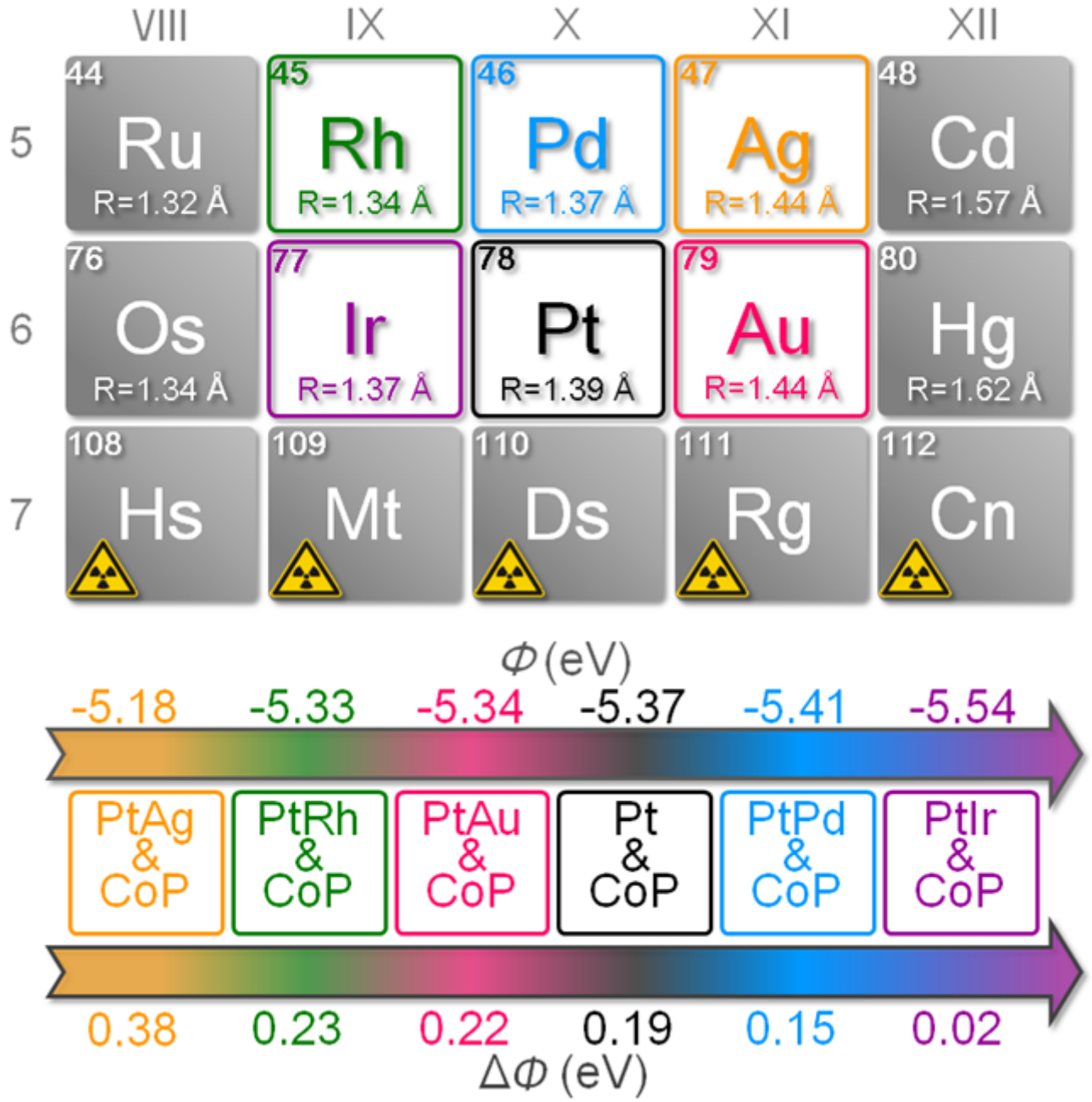

Figure 2

Design of PtM/CoP model catalysts with the controllable ΔΦ.

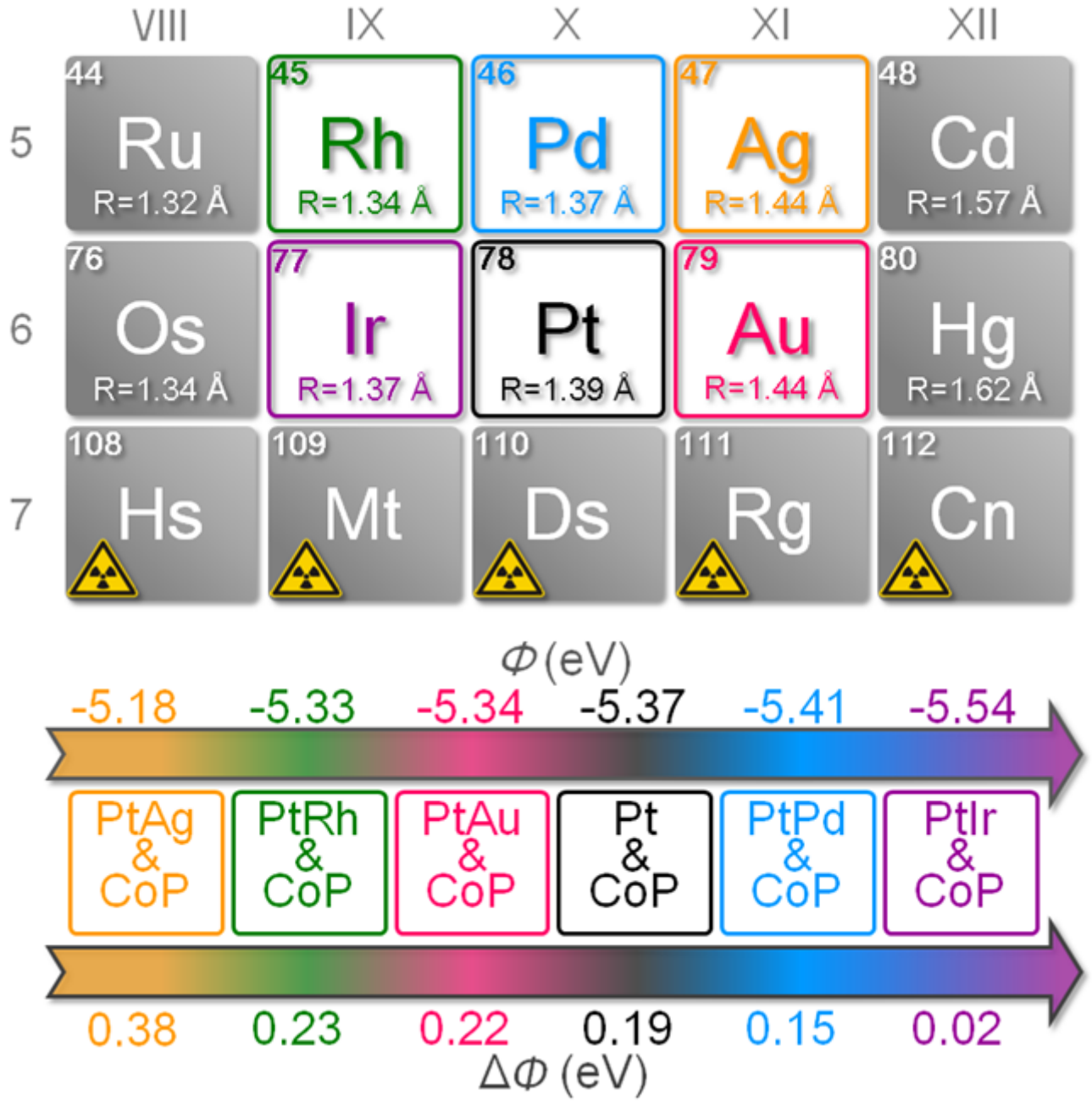

Figure 2

Design of PtM/CoP model catalysts with the controllable ΔΦ.

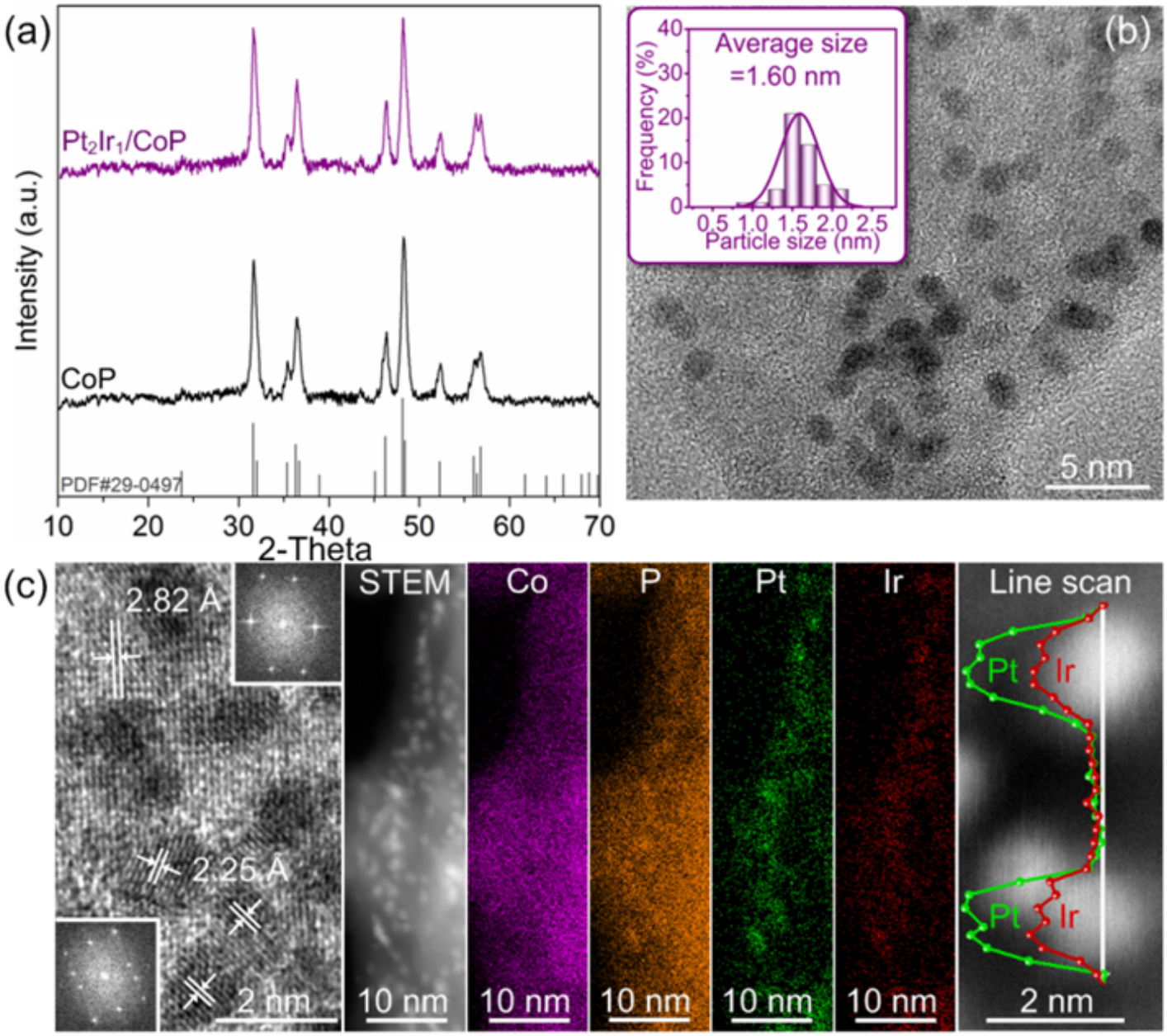

Figure 3

Characterizations for a paradigm of PtM/CoP catalyst. (a) XRD patterns for the Pt2Ir1/CoP and CoP. (b) TEM images for the Pt2Ir1/CoP. (c) HR-TEM images, elemental X-ray mapping and line scan for the Pt2Ir1/CoP.

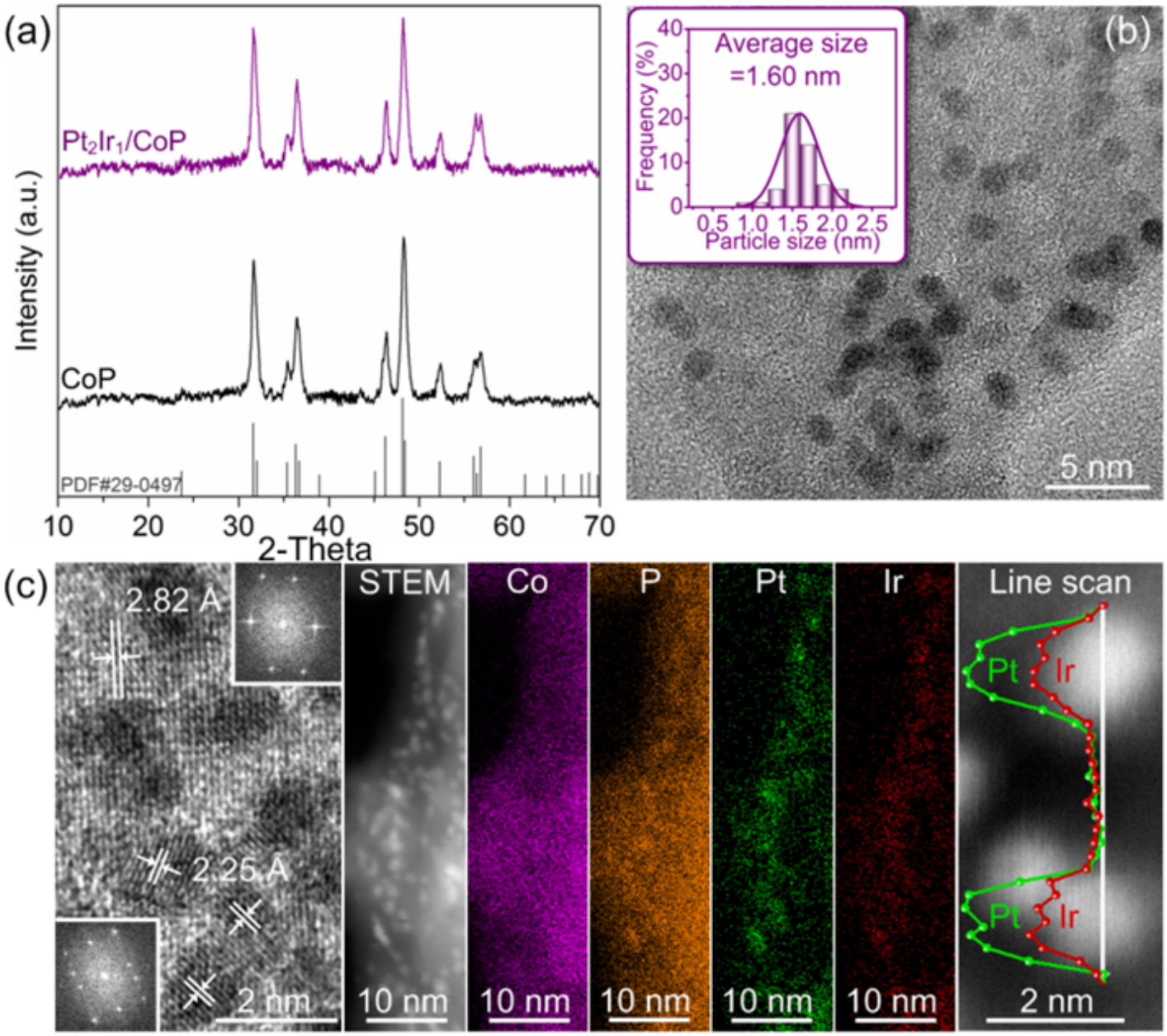

Figure 3

Characterizations for a paradigm of PtM/CoP catalyst. (a) XRD patterns for the Pt2Ir1/CoP and CoP. (b) TEM images for the Pt2Ir1/CoP. (c) HR-TEM images, elemental X-ray mapping and line scan for the Pt2Ir1/CoP.

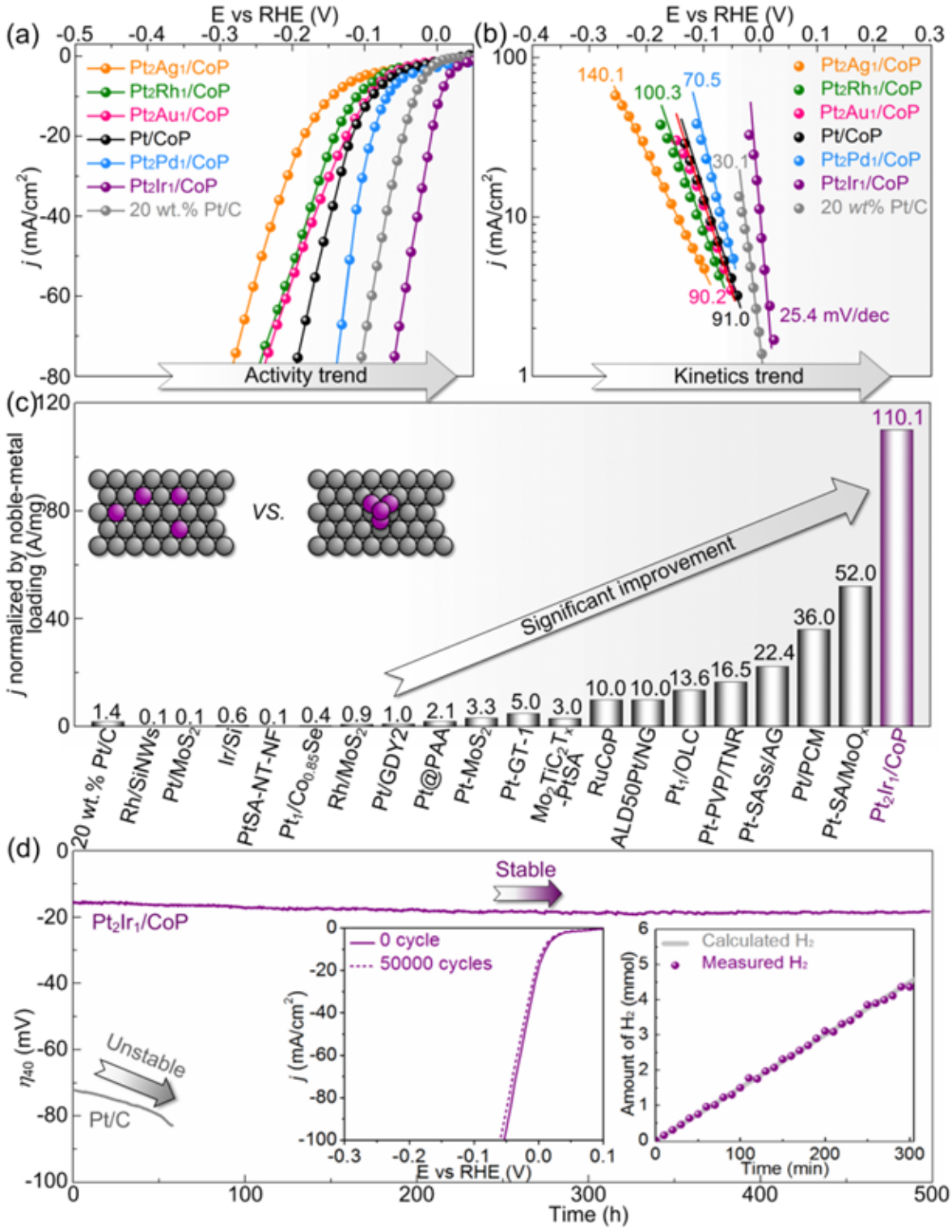

Figure 4

Catalytic evaluation of PtM/CoP with a total metal loading of 1.0 wt.% in 0.5 M H2SO4. (a) LSV curves of various Pt2M1/CoP and Pt/CoP catalysts (1.0 wt.%) and Pt/C (20 wt.%) benchmarks. (b) LSV–derived Tafel plots for various catalysts. (c) Comparisons of the noble-metal utilization activity of Pt2Ir1/CoP (1.0 wt.%) for HER with those of other well-known noble-metal based catalysts, especially the single-atom Pt

catalysts.21,23,26,38-51 (d) Catalytic durability of Pt2Ir1/CoP (1.0 wt.%) through a time-overpotential profile at 40 mA•cm−2. Insets are cycle performance of LSV curves and Faradic efficiency.

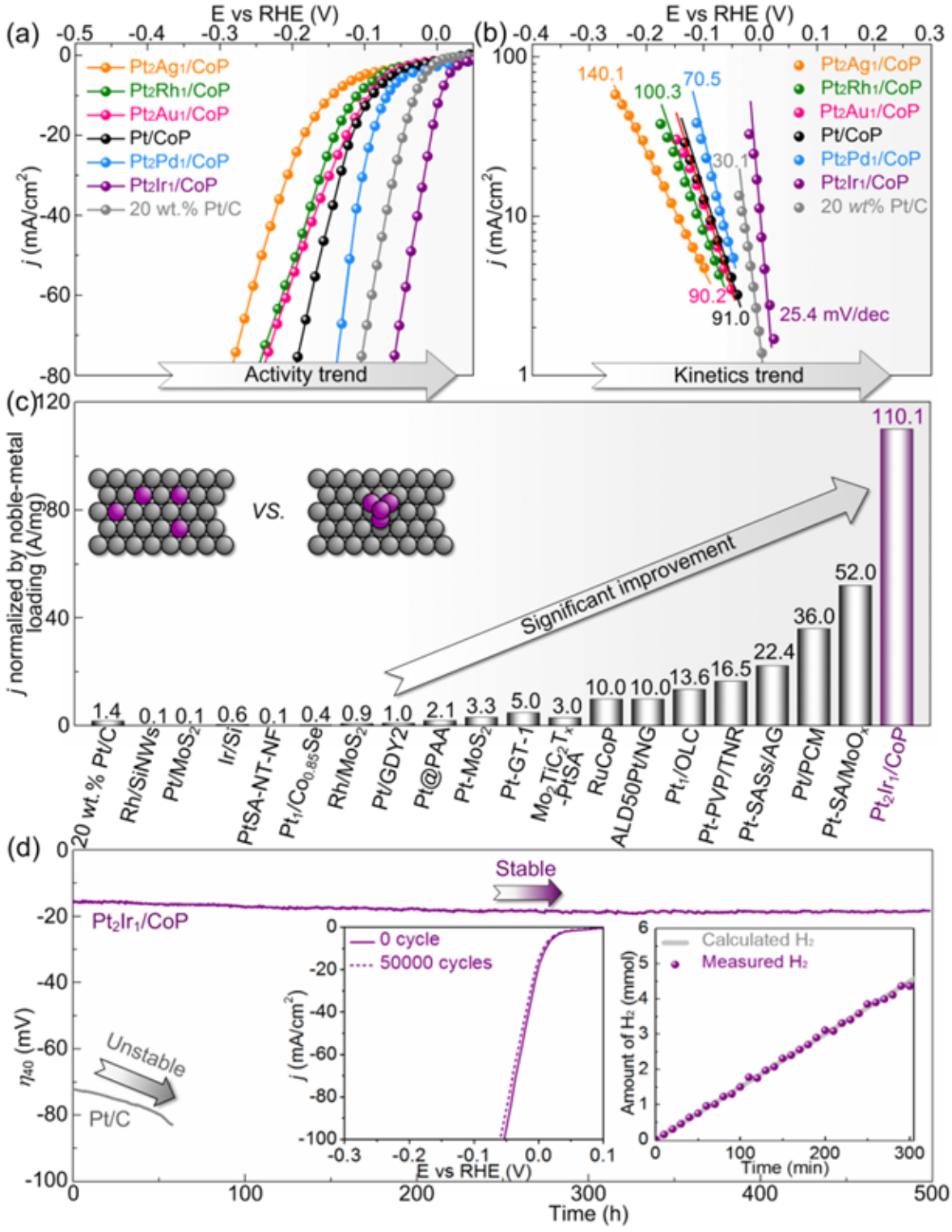

Figure 4

Catalytic evaluation of PtM/CoP with a total metal loading of 1.0 wt.% in 0.5 M H2SO4. (a) LSV curves of various Pt2M1/CoP and Pt/CoP catalysts (1.0 wt.%) and Pt/C (20 wt.%) benchmarks. (b) LSV–derived Tafel plots for various catalysts. (c) Comparisons of the noble-metal utilization activity of Pt2Ir1/CoP (1.0

wt.%) for HER with those of other well-known noble-metal based catalysts, especially the single-atom Pt catalysts.21,23,26,38-51 (d) Catalytic durability of Pt2Ir1/CoP (1.0 wt.%) through a time-overpotential profile at 40 mA•cm−2. Insets are cycle performance of LSV curves and Faradic efficiency.

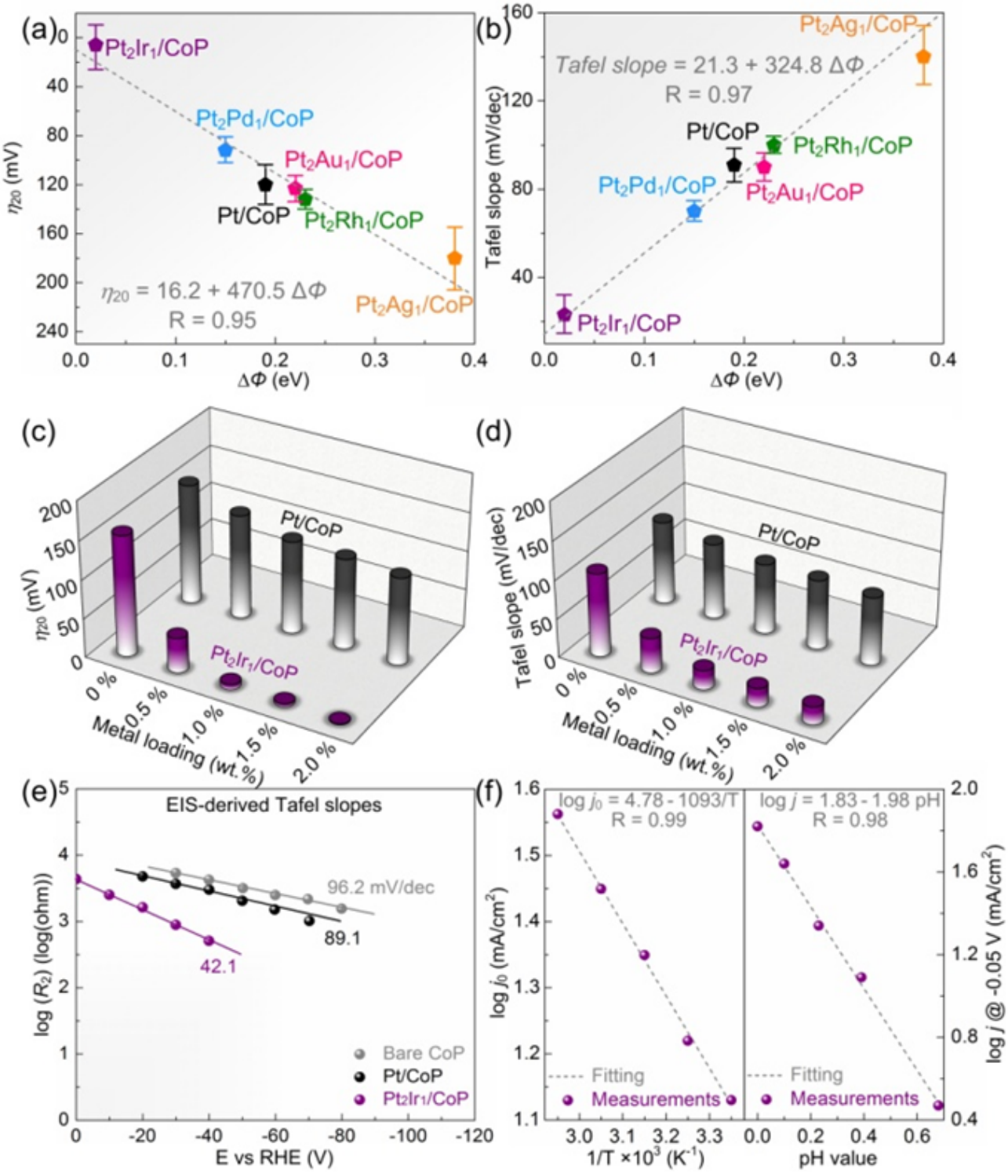

Figure 5

Correlation with intrinsic HER activity of various PtM/CoP model catalysts and their ΔΦ. (a) HER activity trends of 20 as a function of the ΔΦ. (b) Plots of LSV–derived Tafel slope values as a function of the

ΔΦ. Comparisons of 20 (c) and Tafel slope (d) of Pt2Ir1/CoP paradigm with Pt/CoP as positive control catalysts at each metal loading. (e) EIS–derived Tafel plots for Pt2Ir1/CoP paradigm, Pt/CoP benchmark and bare CoP obtained from the H* adsorption resistance R2. (f) Typical Arrhenius plots (left) and plots of log j at -0.05 V (vs. RHE) vs. pH (right) for Pt2Ir1/CoP paradigm.

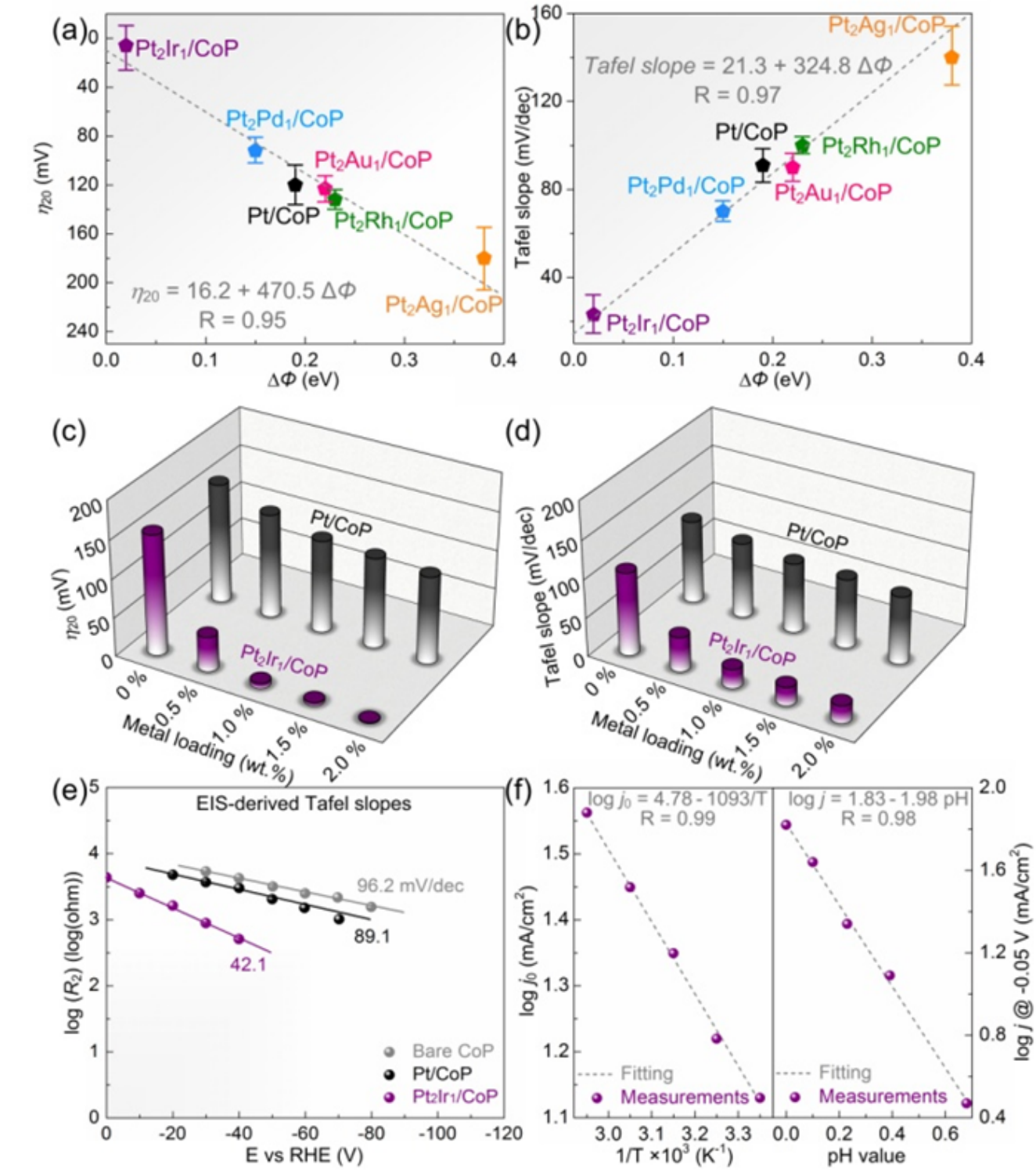

Figure 5

Correlation with intrinsic HER activity of various PtM/CoP model catalysts and their ΔΦ. (a) HER activity trends of ⍰20 as a function of the ΔΦ. (b) Plots of LSV–derived Tafel slope values as a function of the ΔΦ. Comparisons of ⍰20 (c) and Tafel slope (d) of Pt2Ir1/CoP paradigm with Pt/CoP as positive control catalysts at each metal loading. (e) EIS–derived Tafel plots for Pt2Ir1/CoP paradigm, Pt/CoP benchmark and bare CoP obtained from the H* adsorption resistance R2. (f) Typical Arrhenius plots (left) and plots of log j at -0.05 V (vs. RHE) vs. pH (right) for Pt2Ir1/CoP paradigm.

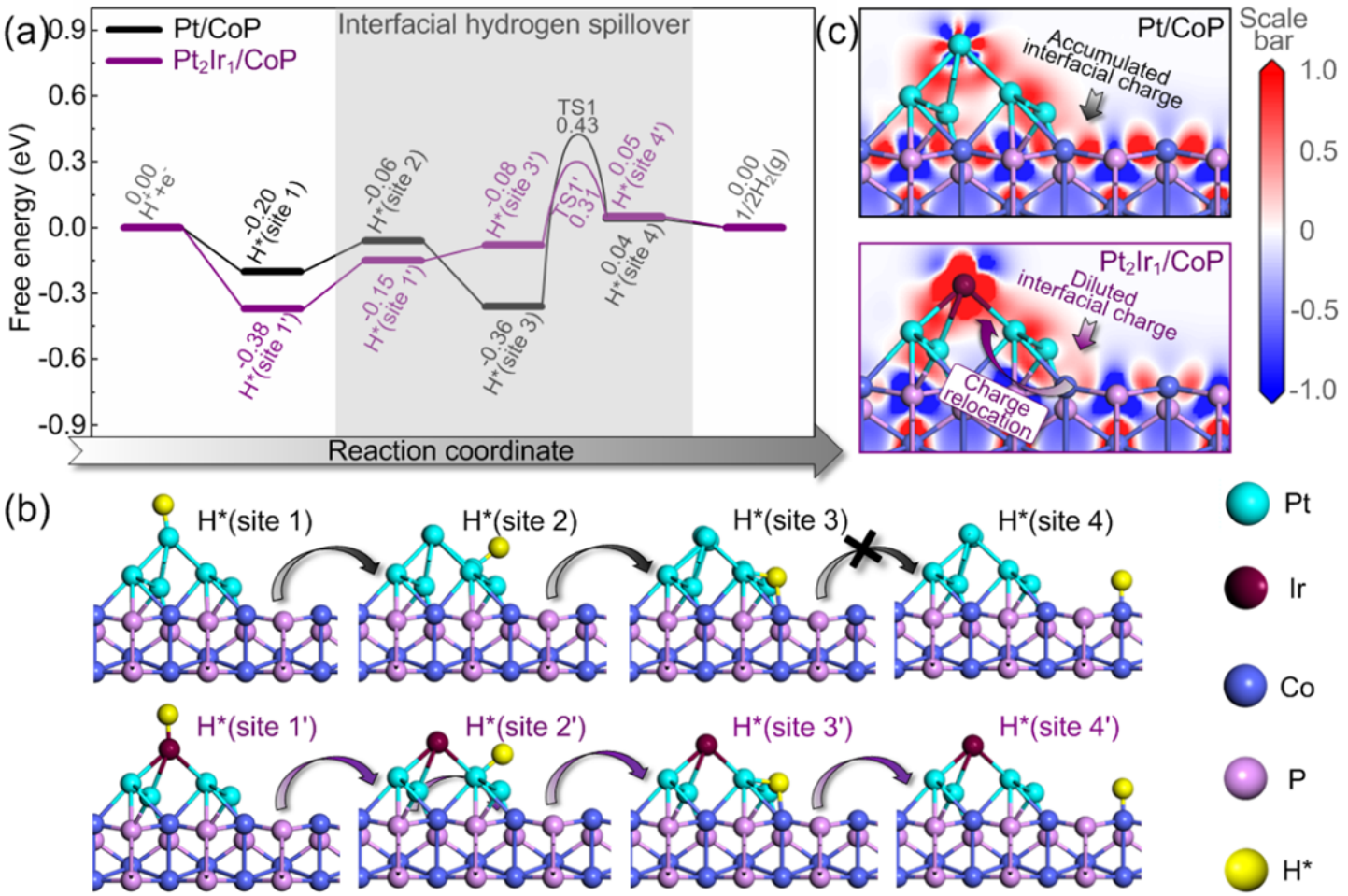

Figure 6

Theoretical modelling. (a) Calculated free energy diagram for HER on Pt2Ir1/CoP paradigm and Pt/CoP benchmark. (b) The optimized H* adsorption structures at various sites. (c) Electron density difference map of interfaces, where a loss of electrons is indicated in blue and electron enrichment is indicated in red.

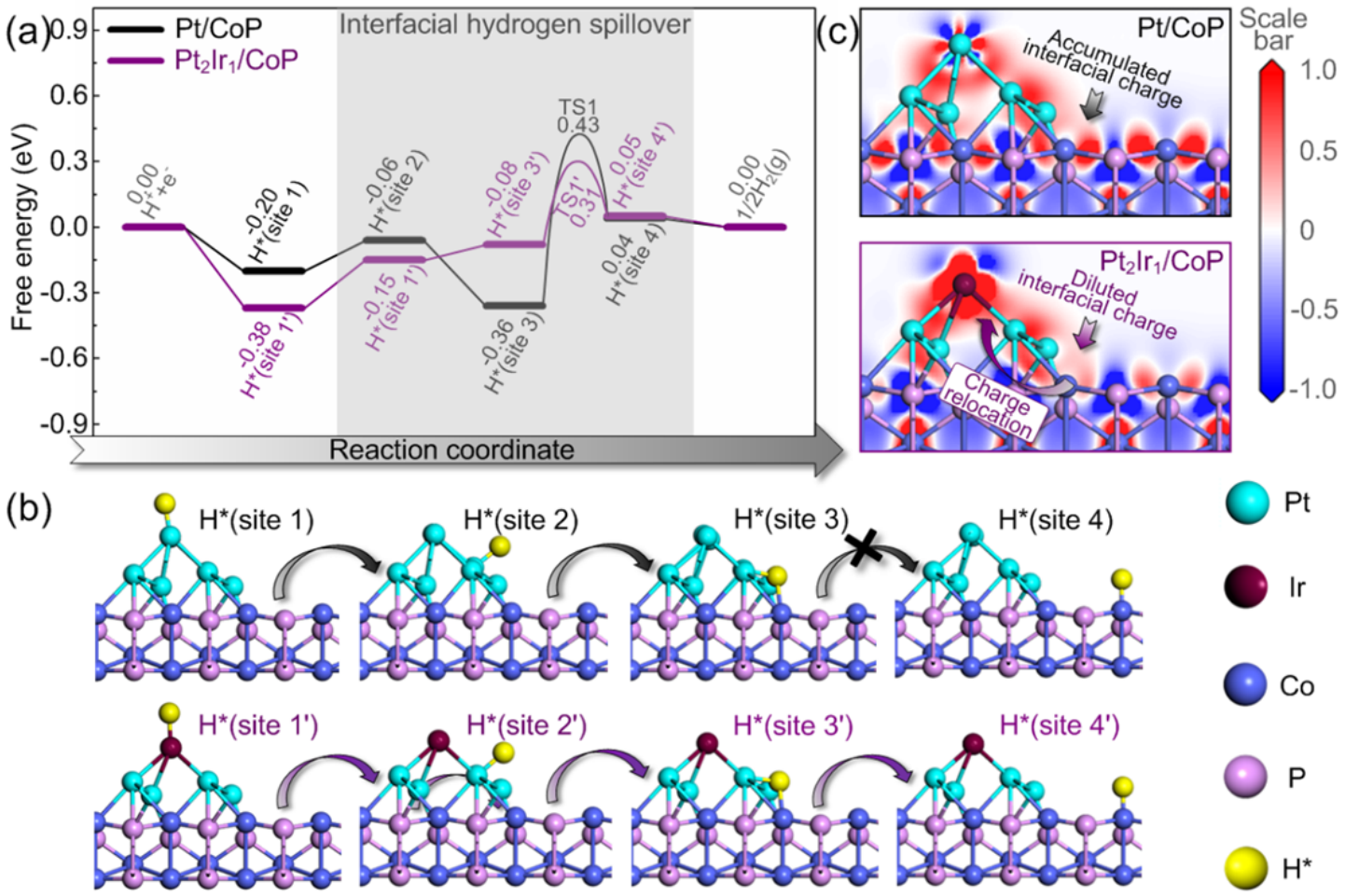

Figure 6

Theoretical modelling. (a) Calculated free energy diagram for HER on Pt2Ir1/CoP paradigm and Pt/CoP benchmark. (b) The optimized H* adsorption structures at various sites. (c) Electron density difference map of interfaces, where a loss of electrons is indicated in blue and electron enrichment is indicated in red.

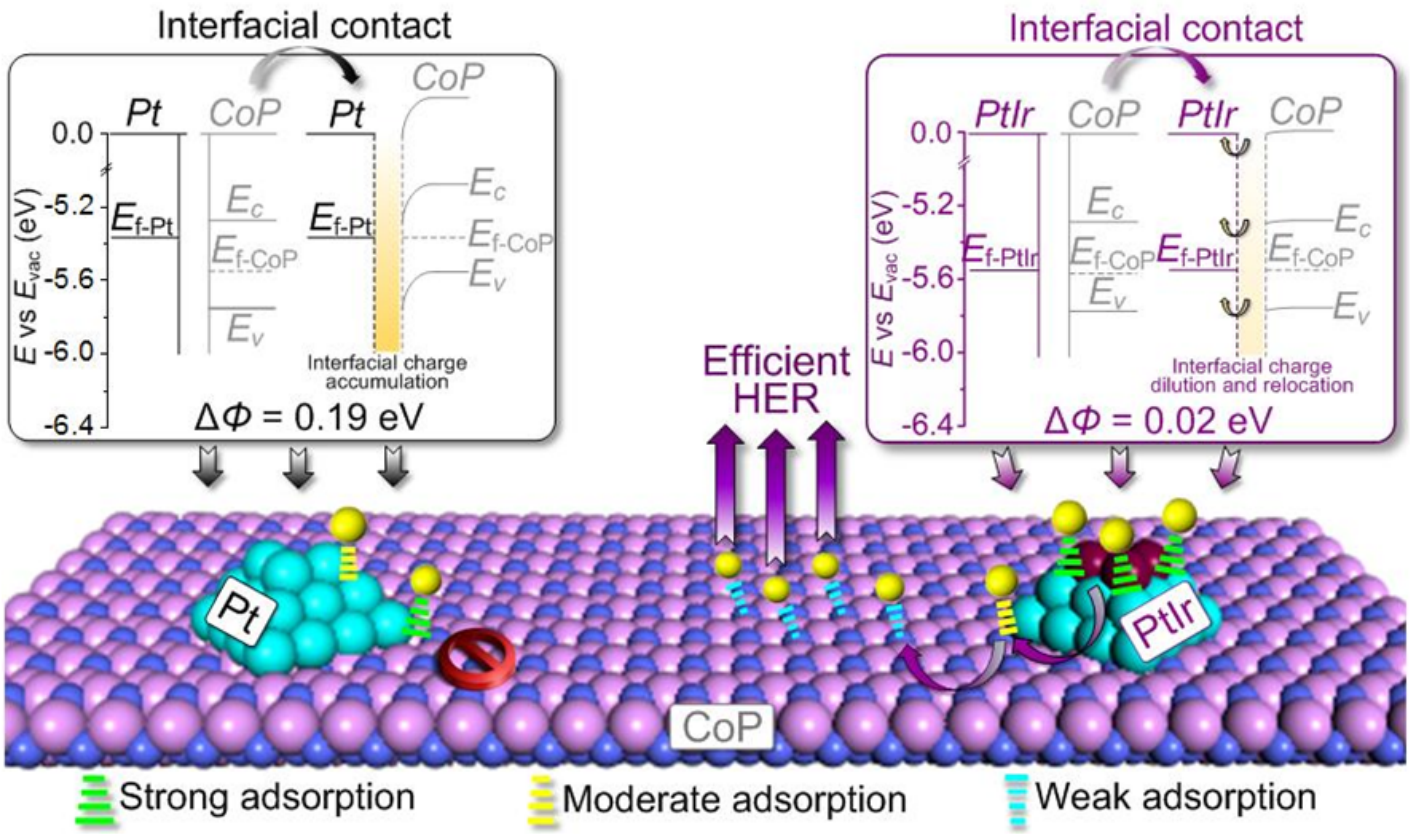

Figure 7

Proposed nature of the ΔΦ on the hydrogen spillover phenomenon in HSBB catalysts.

Interfacial contact
Pt
CoP
Pt
CoP
0.0
-5.2
-5.6
-6.0
-6.4
E vs Evac (eV)
Ef-Pt
Ec
Ef-CoP
Ev
Interfacial charge accumulation
ΔΦ = 0.19 eV
Interfacial contact
PtIr
CoP
PtIr
CoP
Ef-PtIr
Interfacial charge dilution and relocation
ΔΦ = 0.02 eV
Efficient HER
Pt
PtIr
CoP
Strong adsorption
Moderate adsorption
Weak adsorption

Figure 7

Proposed nature of the ΔΦ on the hydrogen spillover phenomenon in HSBB catalysts.

Supplementary Files

This is a list of supplementary files associated with this preprint. Click to download.

- SIPtIrCoP.docx
- SIPtIrCoP.docx